Front. Earth Sci. 2022, 16(4): 1025–1039
https://doi.org/10.1007/s11707-022-0972-7

RESEARCH ARTICLE

Evaluation on the applicability of ERA5 reanalysis dataset to tropical cyclones affecting Shanghai

Zhihui HAN[1], Caijun YUE (✉)[2,1], Changhai LIU[3], Wen GU[1], Yuqi TANG[1], Yongyu LI[4]

1 Shanghai Ecological Forecasting & Remote Sensing Center, Shanghai 200030, China
2 Shanghai Marine Meteorological Center, Shanghai 200030, China
3 National Center for Atmospheric Research, Boulder, CO 80305, USA
4 Shanghai Baoshan Meteorological Bureau, Shanghai 201900, China

Abstract Based on the 16 historical tropical cyclones (TCs) affecting Shanghai from 2007 to 2019, the suitability of ERA5 for studying TCs affecting Shanghai is systematically evaluated from the perspective of TC track, intensity, 10-m and upper-level wind, using TC best-track data of China Meteorological Administration and surface observations and sounding data. Corresponding to tropical storm (TS), strong tropical storm (STS), typhoon (TY), strong typhoon (STY) and super typhoon (SuperTY), the median TC track bias is 68.1, 52.9, 42.5, 25.4, and 18.2 km, respectively, the median maximum 10-m wind speed ($VMAX_{10m}$) bias is –3.7, –6.5, –11.4, –21.7, and –32.2 $m \cdot s^{-1}$, respectively, and the median minimum mean sea level pressure ($MSLP_{min}$) bias is 2.2, 5.6, 8.1, 28.2, and 48.7 hPa, respectively. With the increase of TC intensity, the median TC track bias decreases, while the median $VMAX_{10m}$ and $MSLP_{min}$ bias increase. In general, $VMAX_{10m}$ in ERA5 is lower than observed, and $MSLP_{min}$ is larger than observed. Under influence of TS, STS, TY and STY, the median 10-m wind speed (V_{10m}) bias in the city is 3.2, 4.2, 4.7, and 5.4 $m \cdot s^{-1}$, respectively, and is 4.4–5.2 $m \cdot s^{-1}$ near the east coast, respectively. V_{10m} is mostly biased high, showing an "M" type pattern with the distance between TC and Shanghai. The median 10 m wind direction (WD_{10m}) bias is in a range of –7° to +7°. The median upper-level wind speed (V_{upper}) bias decreases with height, with a maximum of ~5 $m \cdot s^{-1}$ at 975 hPa. Below 900 hPa V_{upper} in ERA5 is typically larger than the radiosonde observation, and its mean bias error (MBE) increases with TC intensity. The upper-level wind direction (WD_{upper}) matches the sounding data well, with a maximum bias of a few degrees only. The results provide a reference for the application of ERA5 to coastal cities affected by TCs.

Received September 27, 2021; accepted January 17, 2022

E-mail: yuecaijun2000@163.com

Keywords ERA5 reanalysis, tropical cyclone, wind field, urban

1 Introdution

Reanalysis products assimilate a large number of satellite data and conventional ground-based and air-borne observation data, providing complete spatial and temporal coverage over long time periods (Thorne and Vose, 2010; Schenkel and Hart, 2012). They can effectively compensate for the deficiencies of observation data under the influence of tropical cyclones (TCs), and are useful tools for studying large-scale weather systems such as TCs (Maloney and Hartmann, 2000a, 2000b). At present, the commonly used reanalysis datasets are as follows: the European Center for Medium-Range Weather Forecasts (ECMWF) Reanalysis-40 (ERA-40) (Uppala et al., 2005), Internal Reanalysis (ERA-I) (Dee et al., 2011) and the fifth generation reanalysis product (ERA5) (Hersbach et al., 2020); the Japanese 55-year and 25-year Reanalysis (JRA-55, JRA-25) by Japanese Meteorological Agency (JMA) and Central Research Institute of Electric Power Industry (Onogi et al., 2007; Kobayashi et al., 2015); the National Centers for Environmental Prediction (NCEP) Climate Forecast System Reanalysis (CFSR) (Saha et al., 2010); the National Aeronautics and Space Administration (NASA) Modern-Era Retrospective Analysis for Research and Applications (MERRA) (Rienecker et al., 2011) and the following version 2 (MERRA-2) (Bosilovich et al., 2015), and so on. As one of the high impact weather systems, TCs often cause natural disasters such as floods and damaging winds, and reanalysis datasets have been widely used for their study (e.g. Hart et al., 2007; Scoccimarro et al., 2012; He et al., 2020; Geetha and Balachandran, 2020; Xi et al., 2020; Tu et al., 2021).

However, owing to the usage of different numerical models, assimilation schemes and assimilation data sources, reanalysis datasets from various institutions often perform discriminatively in reproducibility of TCs and their atmospheric environment (Zarzycki et al., 2021). Therefore, it is of great significance to evaluate the TC representation in reanalysis datasets (Knutson et al., 2008; Murakami, 2014).

Hatsushika et al. (2006) reported that JRA-25 and ERA-40 represent the TC track and frequency in the western North Pacific, the eastern North Pacific and the North Atlantic discrepantly, and JRA-25 performs better in general. Manning and Hart (2007) evaluated the TC intensity and structure in ERA-40. Along with the steady increase and update of reanalysis datasets, more and more research compared the performance of different reanalysis datasets in TC representation. Schenkel and Hart (2012) analyzed TC location and intensity in ERA-40, ERA-I, CFSR, JRA-25 and MERRA, and found obvious differences are present among these datasets, and CFSR and JRA-25 perform best, but the intensity is significantly underestimated. Murakami (2014) showed that JRA-55, JRA-25, ERA-40, ERA-I, CFSR and MERRA provide a reasonable TC distribution and generation, but underestimate TC intensity. Hodges et al. (2017) also identified and compared TCs in ERA-40, ERA-I, CFSR, JRA-25, MERRA, and MERRA-2, and concluded that the largest uncertainties exist in weak TCs, and high-resolution reanalysis datasets are superior. Schenkel et al. (2017) further evaluated the outer TC size and structure in CFSR, ERA-I, JRA-55, and MERRA2, demonstrating a close match to QuikSCAT tropical cyclone radial structure dataset. In closing, previous studies showed that reanalysis datasets perform differently in TC track, genesis and size, and all underestimate TC intensity (Zick and Matyas, 2015; Zarzycki et al., 2021), which can only be alleviated with more frequent, higher density observation and finer resolution.

In 2016, the fifth-generation reanalysis dataset ERA5 was launched by ECMWF, benefiting from the advanced achievements in the model physics, core dynamics and data assimilation (Hersbach et al., 2020). ERA5 provides 0.25° and hourly global geophysical parameters with 137 vertical levels. Its significant resolution improvement allows much more details of TCs to be depicted both in space and in time (Hersbach et al., 2020). For example, for TC Florence, which hit the east coast of the USA in September 2018, the central pressures in ERA5 are lower than those in ERA-I, closer to those of ECMWF operational HRES analysis (Hersbach, 2019). For the storm Lothar in December 1999, ERA5 captures its detailed and rapid evolution, providing a maximum wind gust comparable to the observation (Hersbach et al., 2020). Malakar et al. (2020) evaluated the TC track, intensity and structure over the North Indian Ocean in ERA5 and ERA-I, GFS, JRA-55, CFSR, MERRA2, and found that ERA5 outperforms the others. A comparison between ERA5, CFSR, ERAI, and a mixed reanalysis-observation dataset, the Cross Calibrated Multi-Platform (CCMP) (Wentz et al., 2015), by Bian et al. (2021) showed that ERA5 reproduces stronger TC wind, with a more realistic outer TC size. Of note is that the previous work focused on TCs over the ocean. Over land the surface-air interaction is very different from that over water. It is a common practice to exclude data over land points when calculating mean wind field of TCs using reanalyzes (e.g., Schenkel et al., 2017; Bian et al., 2021). Especially, the impact of complex urban rough surface could complicate the TC representation in reanalysis data, and thus a systematic examination is much needed on the suitability of ERA5 for studying TCs affecting megacities.

Shanghai is located on the east coast of China, surrounded by water on three sides. TC is one of the high impact weather systems that affects Shanghai in summer, with an average of about two each year (Yue et al., 2019). In recent years, global warming has led to an increasement of extreme weather, TC intensity and the proportion of strong TCs that land in China (An et al., 2013). As one of the most populous cities in China, Shanghai is particularly vulnerable to TC damages and has suffered tremendous economic losses. For example, TC Haikui in 2012 disrupted the transportations, with railway, subway and Maglev systems being suspended, blew down more than 30000 trees, damaged numerous large billboards and tens of thousands of vegetable and fruit greenhouses, and incurred an agricultural production loss of nearly 500 million yuan. However, the TC forecasting in Shanghai still presents a great challenge, and our understanding of its physical processes and fine-scale structures has been limited by insufficient observational data and coarse-resolution reanalysis data. Considering its high spatial and temporal resolution, ERA5 thus provides an opportunity for us to improve our knowledge of TCs affecting Shanghai. Therefore, it is important and of practical value to perform a systematic evaluation on ERA5's reproducibility of TCs that traverse Shanghai or nearby regions.

In this paper, the representation of historical TCs in ERA5 that affect Shanghai during 2007–2019 is investigated in terms of track, intensity, surface and upper-level wind. The primary purpose is to quantify the applicability of ERA5 to the research of TCs affecting Shanghai. This paper is organized as follows: Section 2 introduces the ERA5 data, various observational data, and analysis method; Section 3 evaluates the TC track and intensity; Section 4 evaluates the 10-m and upper-level wind during the TC passage; and a summary and discussion are given in Section 5.

2 Data and methods

2.1 Data

The reanalysis data of ERA5 used in this paper are downloaded from the official website of ECMWF. The acquired data include the hourly 0.25°-resolution 10-m wind field, mean sea level pressure, and upper wind at 26 pressure levels between 975 and 100 hPa.

The influence of TC on Shanghai is determined on the base of the wind field influence. Specifically, during the passage of TC, when the maximum 10-min average wind speed at two or more Automatic Weather Stations (AWSs) in Shanghai (Fig. 1) is greater than or equal to 10.8 $m \cdot s^{-1}$, the TC is considered to have an impact on Shanghai (Xu, 2005). According to this standard, there were 16 historical TCs affecting Shanghai from 2007 to 2019 as displayed in Table 1 and Fig. 2. The People's Square (121.47°E, 31.23°N) (Fig. 1) is used to represent Shanghai's location. As such, a TC with its center latitude located to the south (north) of the People's Square is treated as being located to the south (north) of Shanghai.

The TC best-track data used to evaluate TC track and intensity in ERA5 is from Shanghai Typhoon Institute of China Meteorological Administration (Ying et al., 2014), which provides TC location and intensity in the western North Pacific and South China Sea at 6-hour intervals. TC intensity is stratified according to the maximum 2-min average wind speed at 10 m ($VMAX_{10m}$) near the TC center, corresponding to the maximum coastal wind speed for TCs landing in China or the maximum wind speed in a range of 300–500 km from the TC center for TCs located in the South China Sea. According to the national standard of tropical cyclone classification (GB/T 19201-2006), TCs are divided into five categories: tropical storm (TS, 17.2–24.4 $m \cdot s^{-1}$), strong tropical storm (STS, 24.5–32.6 $m \cdot s^{-1}$), typhoon (TY, 32.7–41.4 $m \cdot s^{-1}$), strong typhoon (STY, 41.5–50.9 $m \cdot s^{-1}$) and super typhoon (SuperTY, $\geqslant$51.0 $m \cdot s^{-1}$).

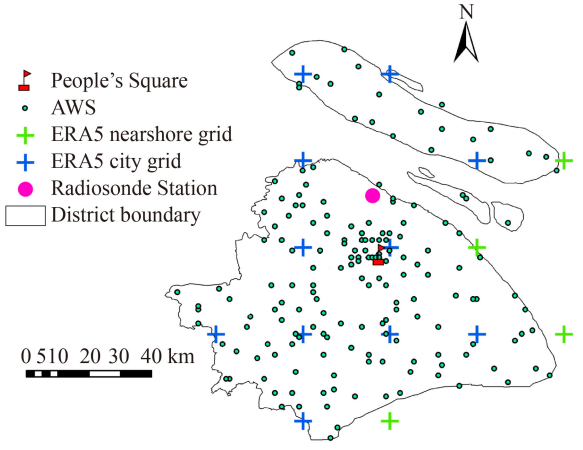

Fig. 1 Location of AWSs, and radiosonde station in Shanghai. "+" symbols stand for ERA5 grid points.

The surface 10-m wind and upper-level wind in ERA5 were validated against the observations at AWSs and Baoshan sounding station in Shanghai (Fig. 1). AWS observations were made with Vaisala WA 15 wind sensors, with a sampling frequency of 1 min. Baoshan sounding station used GFE(L)-1 sounding balloon and GTS1 digital sonde, with a sampling frequency of 1.2 s. The sounding was acquired twice daily, at 08:00 and 20:00 LST.

2.2 Methods for TC detection and analysis of track and intensity

2.2.1 Track

TC center is theoretically the geometric center of the cyclonic circulation. In the actual operation in best-track, TC center determination is mainly based on meteorological satellite imagery, ground-based radar and ground meteorological observation. TCs in ERA5 were tracked on the basis of the 850-hPa vorticity center location (Lam and Lai, 1994; Chen et al., 2008; Tu and Yao, 2010). The procedure was as follows: 1) calculate the 850-hPa vorticity using the wind data in ERA5; and 2) define the grid point of maximum positive vorticity as the TC center, along with an inspection on whether there is a cyclonic circulation around the maximum vorticity point to eliminate false TC centers.

TC best-track data were taken as true meteorological conditions and used to investigate the representation of

Table 1 Tropical cyclones (TCs) that affected Shanghai during 2007–2019. They were identified based on the maximum 10-min average wind speed at two or more AWSs, which is greater than or equal to 10.8 $m \cdot s^{-1}$

TC code	Name	Time span affecting Shanghai (LST)
1909	Lekima	9 Aug, 12:00–11 Aug, 06:00
1913	Lingling	6 Sep, 18:00–7 Sep, 07:00
1917	Tapah	21 Sep, 11:00–22 Sep, 14:00
1918	Mitag	1 Oct, 11:00–2 Oct, 12:00
1810	Ampil	21 Jul, 23:00–23 Jul, 05:00
1812	Jongdari	3 Aug, 02:00–20:00
1814	Yagi	12 Aug, 11:00–13 Aug, 20:00
1818	Rumbia	16 Aug, 09:00–18 Aug, 16:00
1614	Meranti	15 Sep, 16:00–16 Sep 20:00
1509	Chan-hom	10 Jul, 22:00–12 Jul, 15:00
1416	Fung-wong	22 Sep, 08:00–23 Sep, 20:00
1109	Muifa	6 Aug, 20:00–7 Aug, 17:00
0908	Morakot	9 Aug, 20:00–11 Aug, 19:00
0807	Kalmaegi	19 Jul, 08:00–20 Jul, 05:00
0808	Fung-wong	29 Jul, 16:00–31 Jul, 12:00
0713	Wipha	9 Sep, 01:00–20 Sep, 11:00

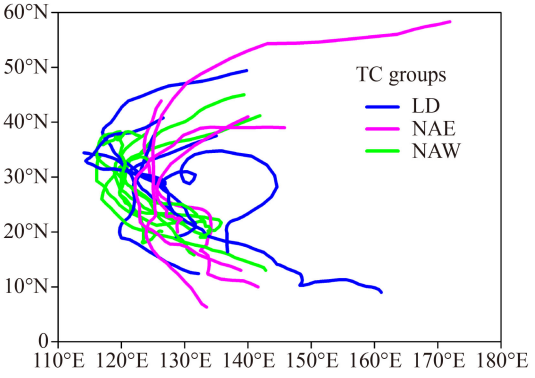

Fig. 2 Best-track of tropical cyclones (TCs) affecting Shanghai during 2007–2019 and three group division: landing in Shanghai (LD), moving northward across the east sea of Shanghai (NAE) and moving northward across the west land of Shanghai (NAW).

TC track in ERA5. To avoid interpolation error, the TC best-track data is compared with ERA5 at 6-hour interval. Note that the horizontal spacing of ERA5 grids is 0.25°. Therefore, if TC track in ERA5 and best-track are compared directly without considering the spatial coverage (0.25° × 0.25°) of ERA5 grids, the difference may be artificially amplified. To eliminate the possible false bias associated with the spatial resolution of ERA5, the following method was adopted in computing the differential longitude (latitude) in TC track, Dist, between the two datasets:

$$\mathrm{Dist}_i = 0 \quad \text{if } |x_{1,i} - x_{2,i}| \leqslant 0.125°, \tag{1}$$

$$\mathrm{Dist}_i = |x_{1,i} - x_{2,i}| - 0.125° \quad \text{if } |x_{1,i} - x_{2,i}| > 0.125°, \tag{2}$$

where i represents either longitude or latitude. The track bias is calculated based on Eqs. (1)–(2).

2.2.2 Intensity

ERA5 $\mathrm{VMAX}_{10\mathrm{m}}$ is defined as the maximum in a range of 20 grids (5°) from the TC center in ERA5. Similarly, ERA5 minimum mean sea level pressure ($\mathrm{MSLP}_{\mathrm{min}}$) is equal to the minimum MSLP in a range of 20 grids (5°) from the TC center. $\mathrm{VMAX}_{10\mathrm{m}}$ and $\mathrm{MSLP}_{\mathrm{min}}$ are compared with their counterparts in best-track to quantify ERA5's performance.

2.3 Method for analysis of wind field in the megacity

2.3.1 10 m wind

Hourly AWS 2-min average wind data in Shanghai are used to evaluate 10-m wind speed ($\mathrm{V}_{10\mathrm{m}}$) and direction ($\mathrm{WD}_{10\mathrm{m}}$) in ERA5. In order to examine the influence of complex underlying surface, the 15 ERA5 grids within Shanghai are classified as either city points (11) or nearshore points (4) (Fig. 1). Each ERA5 grid is paired with the nearest AWS, and $\mathrm{V}_{10\mathrm{m}}$ and $\mathrm{WD}_{10\mathrm{m}}$ are then compared between ERA5 and the AWS observations. Hourly mean bias error (MBE) of $\mathrm{V}_{10\mathrm{m}}$ and $\mathrm{WD}_{10\mathrm{m}}$ is calculated separately for the city and nearshore region. In the following presentation, "city/nearshore $\mathrm{V}_{10\mathrm{m}}$/$\mathrm{WD}_{10\mathrm{m}}$ bias" is used to express the averaged MBE over the city/nearshore grids in the wind field evaluation.

2.3.2 Upper-level wind

Baoshan radiosonde station was matched with the nearest ERA5 grid, and the sounding data acquired at 08:00 and 20:00 Beijing Time each day, were used for the evaluation of upper-level wind speed ($\mathrm{V}_{\mathrm{upper}}$) and direction ($\mathrm{WD}_{\mathrm{upper}}$) at the same time.

3 Evaluation of TC track and intensity

During 2007–2019, a total of 16 TCs are detected, which passed over Shanghai or nearby regions, based on the influence standard in Section 2.1. According to the track location with respect to Shanghai, they are divided into three groups: landing in Shanghai (4 TCs), moving northward across the east sea of Shanghai (5 TCs) and moving northward across the west land of Shanghai (7 TCs) (hereafter LD, NAE and NAW, respectively) (Fig. 2). In this section the ability of ERA5 to represent TC track, $\mathrm{VMAX}_{10\mathrm{m}}$ and $\mathrm{MSLP}_{\mathrm{min}}$, as well as the possible track dependency and influence of underlying surface, will be assessed. The samples for tropical storm (TS), strong tropical storm (STS), typhoon (TY), strong typhoon (STY), and super typhoon (SuperTY), are 213, 93, 92, 38, and 40, respectively.

3.1 Track

The median TC track bias (Fig. 3(a)), corresponding to TS, STS, TY, STY and SuperTY, is 68.1, 52.9, 42.5, 25.4, and 18.2 km, respectively, decreasing with the increase of TC intensity. The average bias of all 16 TCs is 58.3 km. The track MBE is apparently affected by not only the TC intensity but also its position relative to the city (Fig. 3(b)). In particular, significant differences exists for TS and TY, where the MBE of LD TCs is the smallest, followed by NAE and NAW TCs. For the rest of TC categories, the MBE difference is rather small between LD, NAE, and NAW TCs (⩽7 km). From the perspective of underlying surface, track MBE of TCs over ocean is smaller than that over land. For TS, STS, and TY, the MBE difference is 6.8, 11.0, 11.7 km, respectively.

The track bias and its variation with TC intensity could be due to several factors. First, the assimilated observation data are still insufficient to capture the position and propagation of TC (Schenkel and Hart,

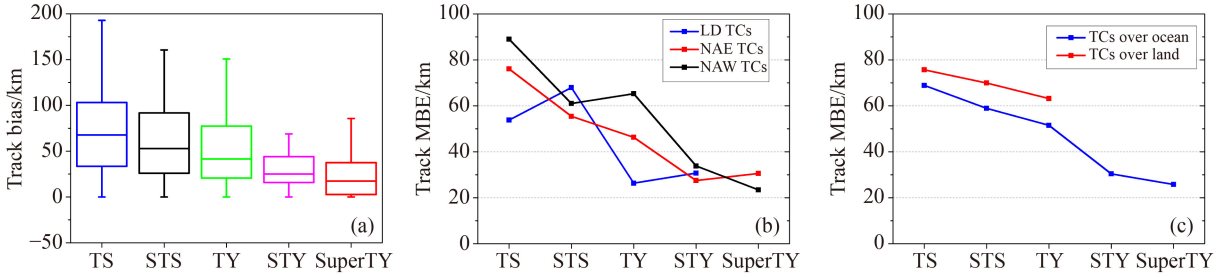

Fig. 3 Median TC track bias (a) of ERA5 with respect to TC best-track data for TS, STS, TY, STY, and SuperTY, with the box indicating the interquartile range (IQR) and the 10th and 90th percentiles given by the whiskers, and TC track MBE for (b) TCs of LD, NAE and NAW, and (c) TCs over ocean and land.

2012). Because TC track in reanalysis is actually a time integral of steering flow, any small deviations in wind field without observation-based corrections may lead to a significant biased track. Second, inaccurate depictions of large-scale systems (such as the subtropical high) that capably modulate TC tracks could be responsible for track errors. Third, stronger TCs have more distinct circulations and structures, and models usually have better skill to reproduce them with a high accuracy. Moreover, the track bias comparison of TCs over different underlying surface indicates that the complicated land surface intensifies the incapability of ERA5 to capture TC location.

3.2 Maximum 10 m wind speed

The representation of TC intensity in ERA5 is first evaluated from the perspective of the maximum surface wind speed $VMAX_{10m}$. 95% of the bias relative to best-track $VMAX_{10m}$ is negative, implying that TC intensity in ERA5 is mostly underestimated. The absolute median $VMAX_{10m}$ bias increases with TC intensity, reaching –3.7, –6.5, –11.4, –21.7, and –32.2 $m \cdot s^{-1}$, corresponding to TS, STS, TY, STY, and SuperTY, respectively (Fig. 4(a)). NAE TCs have the smallest $VMAX_{10m}$ MBE, whereas a comparable MBE exists between LD and NAW TCs (Fig. 4(b)). For all typhoon categories, the absolute MBE of NAE TCs is 5 $m \cdot s^{-1}$ less than that of NAW TCs. The absolute $VMAX_{10m}$ MBE of TCs over ocean and land has slight difference, with a maximum disparity of 1.3 $m \cdot s^{-1}$ for STS.

In all the samples, the maximum $VMAX_{10m}$ in ERA5 is 36.6 $m \cdot s^{-1}$ only reaching the intensity of TY. Therefore, similar to other reanalysis datasets (Schenkel and Hart, 2012; Murakami, 2014; Hodges et al., 2017), ERA5, even with spatial resolution improved to 0.25°, still underestimates the maximum wind speed. This is possibly due to the following factors: 1) the spatial resolution is still insufficient to resolve the complex internal structure of TC; and 2) the biased track could result in a weaker TC than observed if TC in the reanalysis moves into a less favorable environment for development than in reality (Schenkel and Hart, 2012).

3.3 Minimum mean sea level pressure

As well as $VMAX_{10m}$, $MSLP_{min}$ is another oft-used index for TC intensity. There is an 82% probability that the $MSLP_{min}$ difference between ERA5 and best-track is positive, which, along with the low biased $VMAX_{10m}$, indicates a widespread under-representation of TC intensity in ERA5. The median $MSLP_{min}$ bias increases with TC intensity (Fig. 5(a)), similar to the aforementioned correlation between the median $VMAX_{10m}$ bias and TC intensity. For TS, STS, TY, STY, and SuperTY, the median $MSLP_{min}$ bias is 2.2, 5.6, 8.1, 28.2, and 48.7 hPa, respectively. For the three stronger TC categories (i.e., TY, STY, and SuperTY), the MBE of NAE TCs is the lowest, followed by NAW and LD TCs (Fig. 5(b)). In contrast, there is no clear linkage between the bias and the geographical location of TC for the two weaker TC categories (i.e., TS and STS). Similar to $VMAX_{10m}$, the $MSLP_{min}$ MBE of TCs over ocean and land has slight difference, with a maximum disparity of 1.5 hPa for STS.

4 Evaluation of the wind field

To comprehensively evaluate the capability of ERA5 in representing the wind field in Shanghai during the TC passage, the surface and upper-level wind were compared against the AWS and radiosonde observations. The possible connections between the performance of ERA5 and TC intensity, track, location relative to the city, and wind direction were also investigated.

4.1 10-m wind speed

The 10-m wind of ERA5 was analyzed over the city and nearshore region separately. As indicated in the statistics (Fig. 6), the V_{10m} bias from the AWS observations is dominantly positive, with a probability of about 98% for both the city and the nearshore region. The median bias in the city is 3.2, 4.2, 4.7, and 5.4 $m \cdot s^{-1}$, corresponding to TS, STS, TY, and STY, respectively, increasing with TC intensity. In contrast, the median nearshore bias varies between 4.4 and 5.2 $m \cdot s^{-1}$, insensitive to TC intensity.

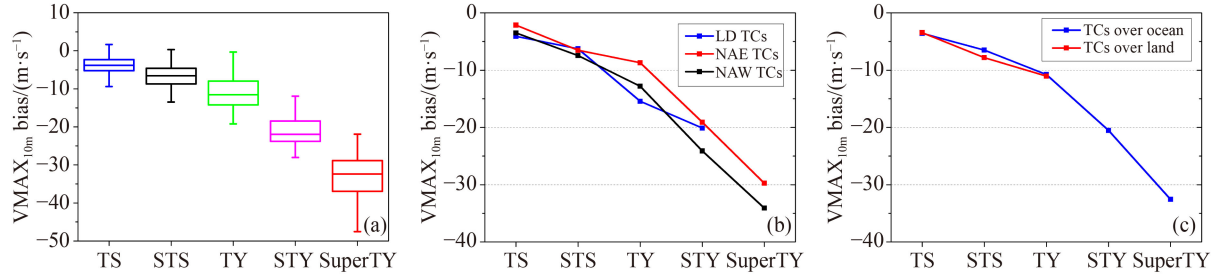

Fig. 4 Median TC $VMAX_{10m}$ bias (a) of ERA5 with respect to TC best-track data for TS, STS, TY, STY, and SuperTY, with the box indicating the IQR and the 10th and 90th percentiles given by the whiskers, and $VMAX_{10m}$ MBE for (b) TCs of LD, NAE, and NAW, and (c) TCs over ocean and land.

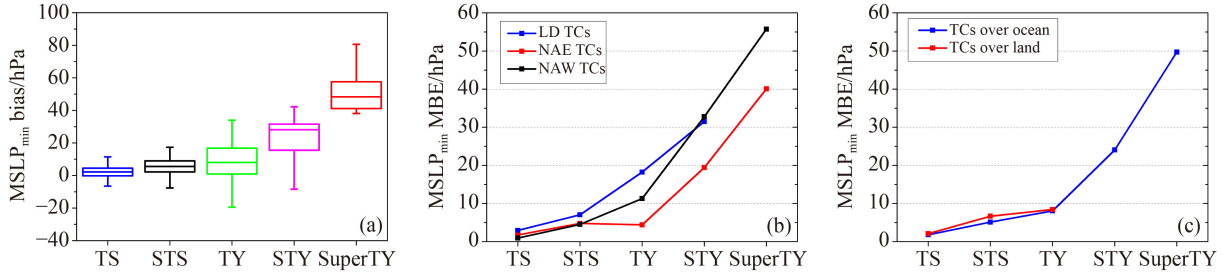

Fig. 5 Median TC $MSLP_{min}$ bias (a) of ERA5 with respect to TC best-track data for TS, STS, TY, STY, and SuperTY, with the box indicating the IQR and the 10th and 90th percentiles given by the whiskers, and $MSLP_{min}$ MBE for (b) TCs of LD, NAE, and NAW, and (c) TCs over ocean and land.

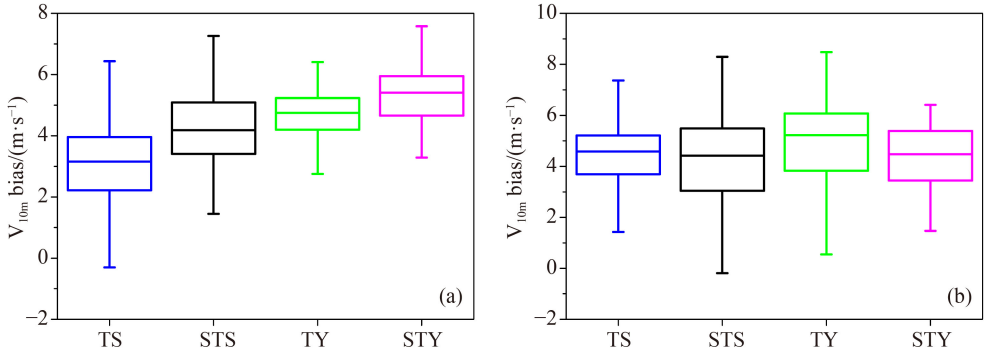

Fig. 6 Median V_{10m} bias relative to the AWS observations for the city, (a) and the nearshore region (b) under influence of TS, STS, TY, and STY, with the box indicating the IQR and the whiskers the 10th and 90th percentiles.

The V_{10m} bias is affected by two factors. One is the ability of ERA5 to reproduce TC intensity. The foregoing analysis has shown that TC intensity in ERA5 is generally weaker, and consequently, V_{10m} of ERA5 should be lower than the observations. Another is whether the effect of urban ground roughness was fully considered in ERA5. It is well known that the surface friction usually reduces the near-surface wind speed. Thus, if ERA5 failed to properly depict the impact of the complex underlying surface in Shanghai, its V_{10m} would be greater than the observations. The fact that V_{10m} in ERA5 is high biased (Fig. 6) suggests that the second factor seemingly plays a major role. The somewhat larger nearshore V_{10m} bias may be attributed to the deficient treatment of coastal surface friction in ERA5 or the less observational data for assimilations in ERA5.

V_{10m} bias of ERA5 depends on the distance between TC and the city as shown in Fig. 7. Negative (positive) abscissa values mean that TCs are located to the south (north) of Shanghai. The larger the absolute values are, the farther TCs are apart from Shanghai. The curves correspond to the median bias as function of the distance from Shanghai. Note that the fragmented curves for TY and STY are associated with the fact that their tracks were beyond 150 km from the city. When TS and STS approach Shanghai from the south, the median V_{10m} bias in the city and nearshore region firstly increases and then decreases, with a peak value around 200 km south of Shanghai. A minimum bias is witnessed when TCs is just situated over the city. Upon leaving from Shanghai, the bias undergoes an increase again, peaks around 200 km north of Shanghai, and then decreases. The “M” type

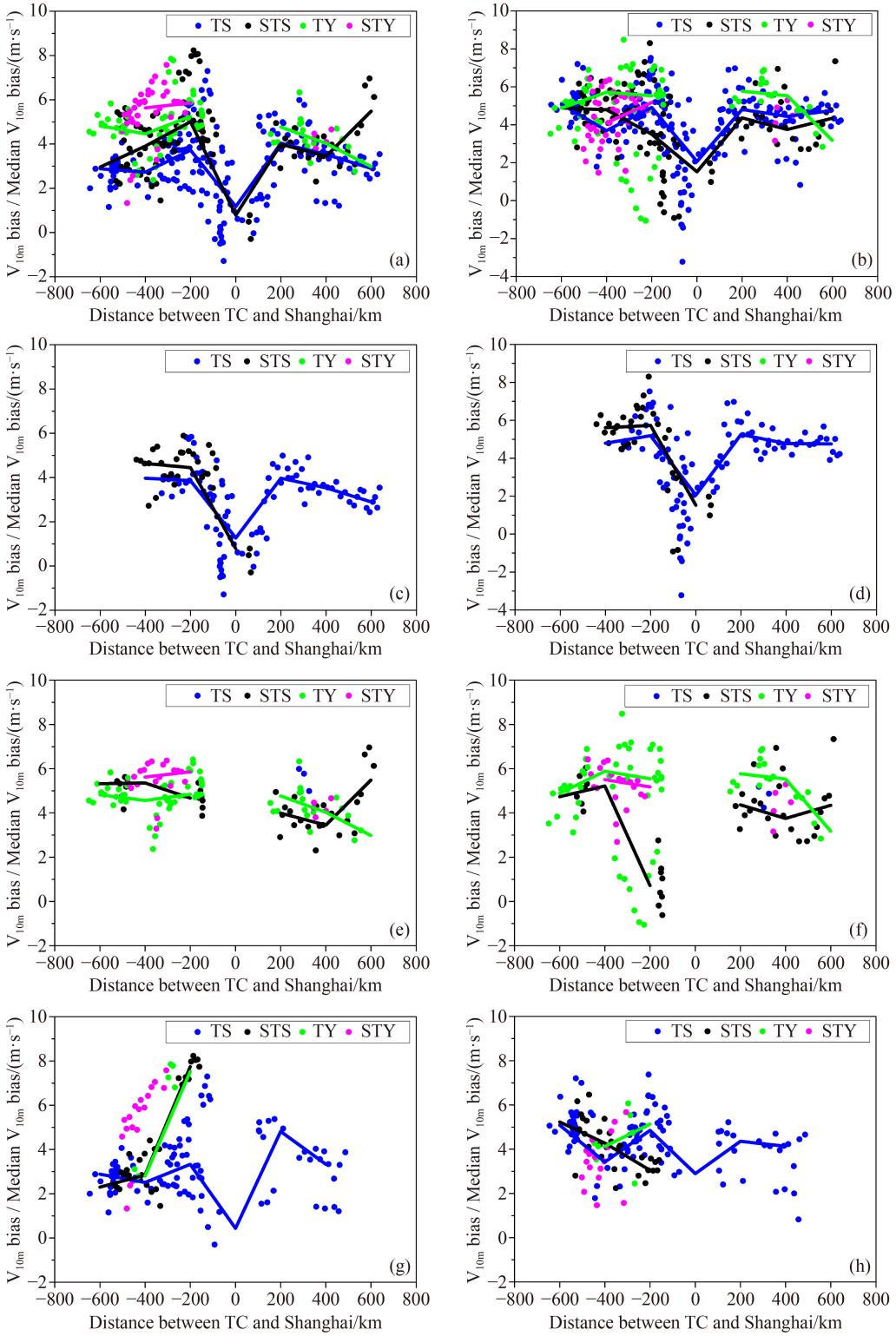

Fig. 7 V_{10m} bias (dot) and Median V_{10m} bias (line) as a function of the distance between TC and Shanghai over city (left) and nearshore region (right) for all 16 TCs (a)–(b), LD TCs (c)–(d), NAE TCs (e)–(f) and NAW TCs (g)–(h). Negative and positive abscissa values correspond to TCs located to the south and north of Shanghai, respectively.

variation of V_{10m} bias may be related to the wind structure characteristics in TC, that is, the wind speed gradually increases from the periphery to the eye wall, and rapidly decreases from the eye wall to the eye. When TCs are beyond 300 km from Shanghai, all city and nearshore V_{10m} bias are positive, that is to say, ERA5 V_{10m} are greater than observations. When TCs are within 300 km from Shanghai, there are some negative V_{10m}

biases with a minimum value of –3.23 $m \cdot s^{-1}$ for the nearshore area and –1.28 $m \cdot s^{-1}$ for the city. These results indicate that when TCs are within 300 km from Shanghai, there are occasions that ERA5 underestimates V_{10m}, perhaps due to the fact that ERA5 did not accurately reproduce the TC internal structure.

About two-thirds of LD TCs consist of TS, with their median V_{10m} biases displaying an "M" type variation with the distance from the city (Figs. 7(c)–7(d)). A widespread overestimate in V_{10m} occurs to both TS and STS, and an occasional underestimate is observed when TCs are within 100 km from Shanghai. The bias varies in a range of –1.28 to 5.88 $m \cdot s^{-1}$ in the city and –3.23 to 8.29 $m \cdot s^{-1}$ in the nearshore area. All NAE TCs are located beyond 150 km away from Shanghai (Figs. 7(e)–7(f)), showing a positive V_{10m} bias almost everywhere except for few occurrences along the coast. The bias is 2.30 to 6.96 $m \cdot s^{-1}$ in the city, and –1.05 to 8.48 $m \cdot s^{-1}$ in the nearshore region. Like LD and NAE TCs, an overestimate in V_{10m} prevails in NAW TCs, and the underestimate only occurs when a TC is close to Shanghai (Figs. 7(g)–7(h)). The bias falls into a range of –0.30 to 8.23 $m \cdot s^{-1}$ in the city, and 0.82 to 7.36 $m \cdot s^{-1}$ in the nearshore region.

In summary, regardless of TC track and intensity, ERA5 overestimates V_{10m}, and the bias features a nonlinear variation with the distance between TC and the city. The city V_{10m} bias increases with TC intensity, while the nearshore bias is larger and has no clear correlation with TC intensity. These V_{10m} deviations may be partially related to the under-representation of urban surface roughness in ERA5.

4.2 10-m wind direction

As shown in Fig. 8, the surface 10-m wind direction (WD_{10m}) in ERA5 was validated against the AWS observations. Herein a positive (negative) difference stands for a clockwise (anticlockwise) bias. A clockwise discrepancy more commonly happens, accounting for a probability of 61.4% in the city and 63.0% in the nearshore region. Corresponding to TS, STS, TY, and STY, the median city WD_{10m} bias is 6.0°, 2.4°, 1.4°, –6.9°, respectively, and the median nearshore bias is 0.8°, 5.7°, 6.5°, –0.7°, respectively. The WD_{10m} representation is closely correlated with how well the underlying surface roughness is parameterized and how well the observed TC rotation is replicated in ERA5. Note that the surface friction reduces wind speed, corresponding to a clockwise rotation bias. Thus, if ERA5 does not fully depict the actual complex urban surface roughness, the TC rotation in ERA5 will be ahead of observation, that is, corresponding to an anticlockwise directional bias. Therefore, on the basis of the above two factors, the clockwise median WD_{10m} bias under the influence of TS, STS and TY is likely attributed to an under-representation of TC rotation in ERA5. In contrast, the anticlockwise bias under the influence of STY may indicate an underestimate of underlying surface roughness, consistent with the high V_{10m} bias in the foregoing analysis. The contrasting WD_{10m} bias for different TC categories is an interesting issue and needs further investigations.

Figure 9 displays the relationship between WD_{10m} bias and TC track. The composite curves of all 16 TCs (Figs. 9(a)–9(b)) indicates a large variation of WD_{10m} bias. When TCs are located to the south of Shanghai, the bias varies between –34.9° and 38.6° for the city, and between –50.1° and 58.6° for the nearshore. When TCs are located to the north of Shanghai, the bias is in a range of –25.8° to 50.3° over the city and –59.0° to 35.9° over the nearshore region. There is no clear correlation between WD_{10m} bias and the distance between TC and Shanghai, and both positive and negative WD_{10m} bias occur when TC approaches and leaves Shanghai. Perhaps due to deficient treatment of urban land surface processes in ERA5, an anticlockwise WD_{10m} bias larger than 20º is witnessed for LD TCs within 100 km from Shanghai (Figs. 9(c)–9(d)). The larger nearshore bias may be indicative of an incomplete depiction of land-sea distributions in ERA5. Under the influence of NAE and NAW TCs or LD TCs beyond 100 km from Shanghai, the anticlockwise WD_{10m} bias is below 20°, and the clockwise bias is relatively large.

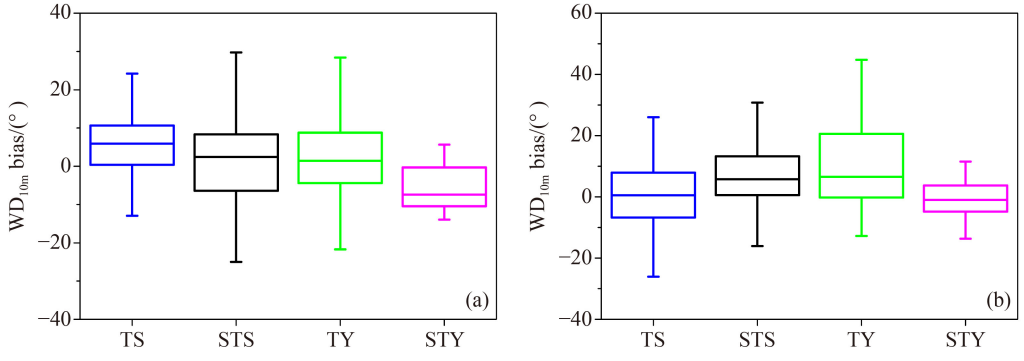

Fig. 8 Median WD_{10m} bias relative to AWS observations for the city (a) and nearshore region (b) under the influence of TS, STS, TY, and STY, with the box indicating the IQR and the whiskers the 10th and 90th percentiles.

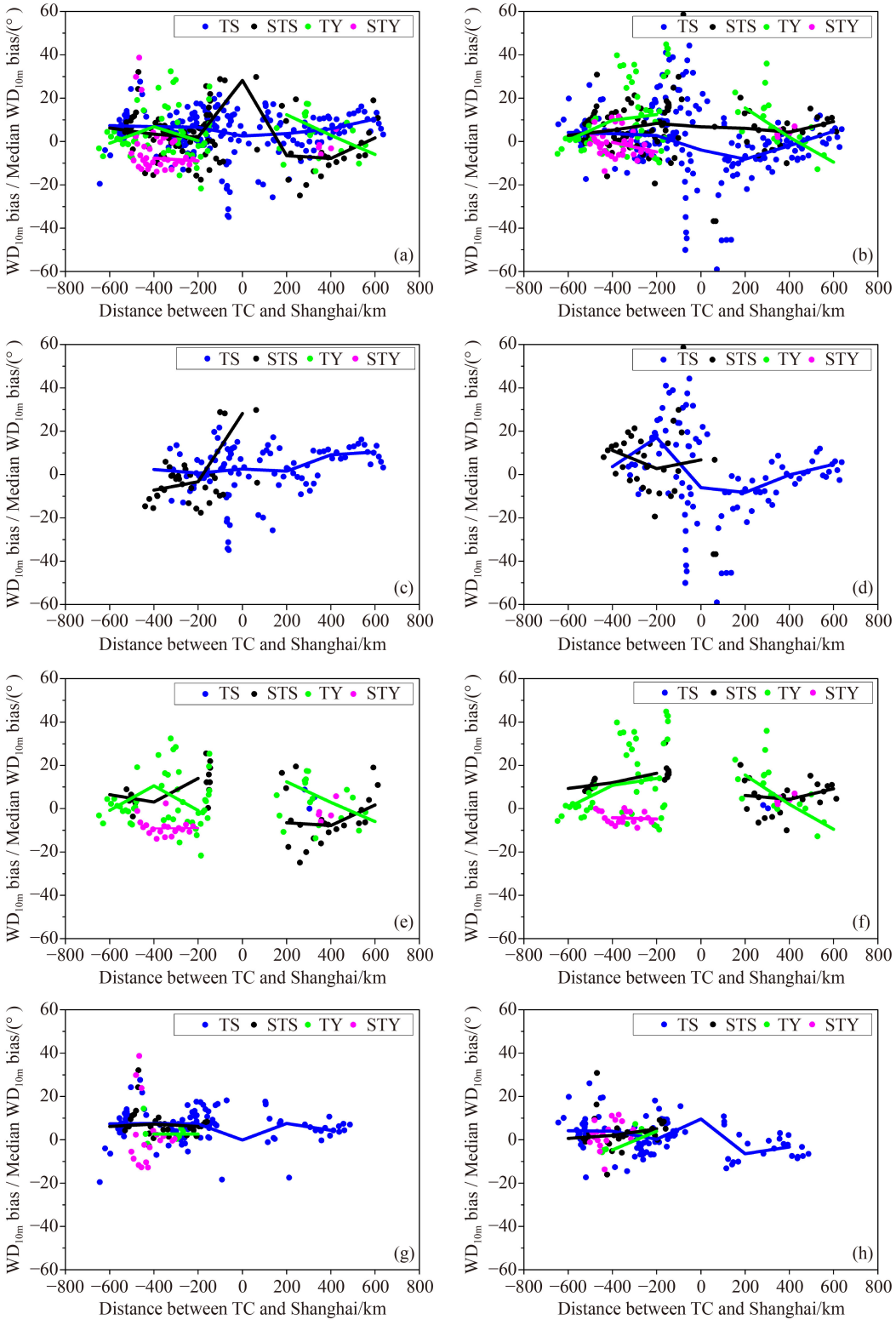

Fig. 9 WD_{10m} bias (dot) and Median WD_{10m} bias (line) as a function of distance between TC and Shanghai over city (left) and nearshore region (right) for all 16 TCs (a)–(b), LD TCs (c)–(d), NAE TCs (e)–(f), and NAW TCs (g)–(h). Negative and positive abscissa values correspond to TCs located to the south and north of Shanghai, respectively.

The relationship between WD_{10m} MBE and wind direction is presented in Fig. 10. As evinced in Figs. 10(a)–10(b), the dominant wind direction for all TC cases is 0°–135° (north wind, northeast wind, east wind, southeast wind), with a proportion of 76.3% and 72.6% for the city and nearshore region, respectively. The same wind

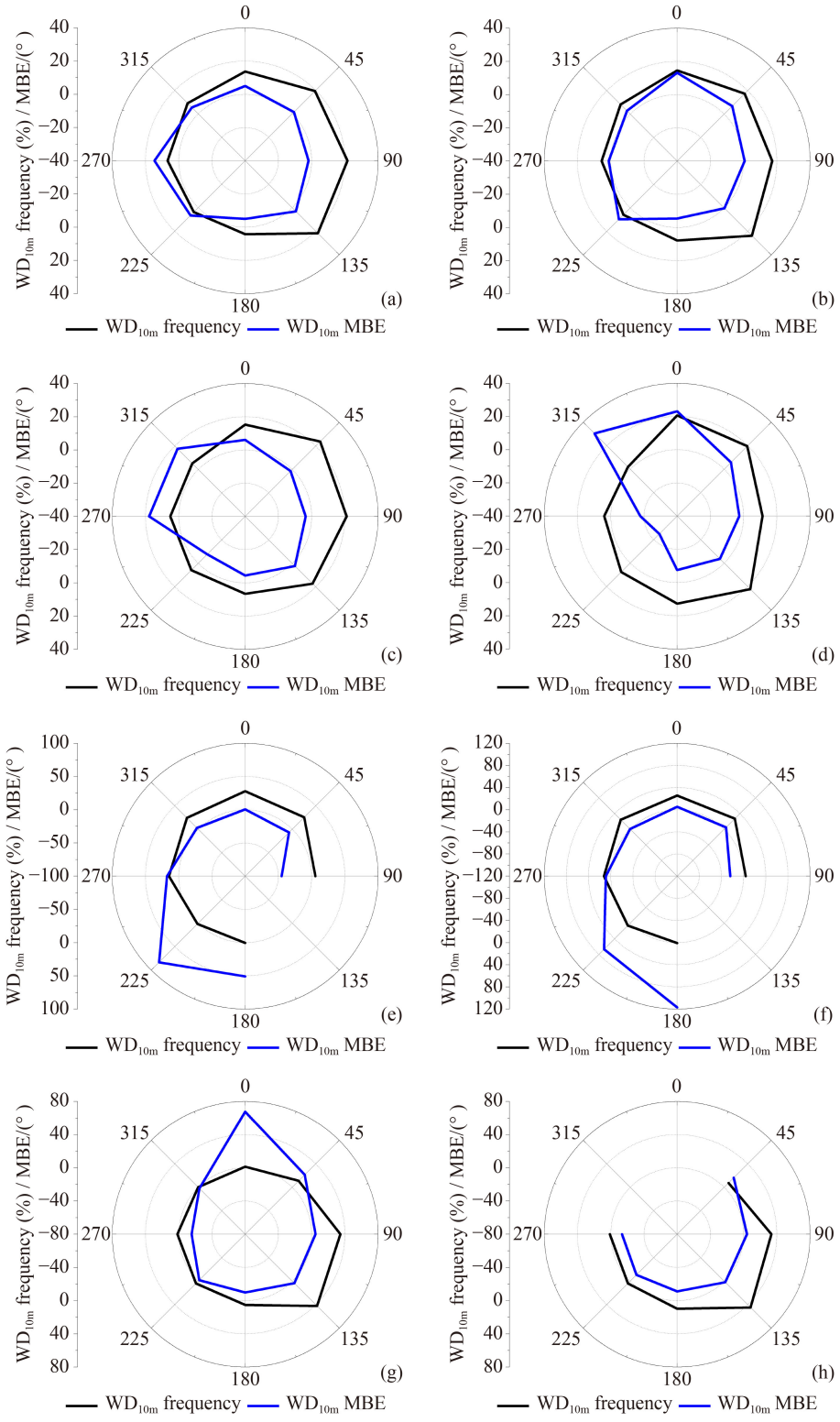

Fig. 10 WD_{10m} frequency and WD_{10m} MBE as a function of wind direction over the city (left) and nearshore region (right) for all 16 TCs (a)–(b), LD TCs (c)–(d), NAE TCs (e)–(f), and NAW TCs (g)–(h).

direction prevails under the influence of LD TCs (Figs. 10(c)–10(d)) and accounts for 77.3% and 73.6% over the city and the nearshore, respectively, in which the WD_{10m} MBE of 90°–135° (east wind, southeast wind) is close to 0°. Under the influence of NAE TCs (Figs. 10(e)–10(f)), the dominant wind direction is 0°–45° and 315° (north wind, northeast wind, northwest wind), with a proportion of 77.2% and 76.7% over the city and

nearshore region, respectively. Under the influence of NAW TCs (Figs. 10(g)–10(h)), the dominant wind direction is 90°–135° (east wind, southeast wind), with a proportion of 76.8% and 77.9% for the city and nearshore region, respectively. For both the NAE and NAW TCs, the WD_{10m} MBE of dominant wind direction is close to 0°. In general, TC track can lead to different dominant 10 m wind directions, and the WD_{10m} bias corresponding to dominant wind directions is relatively small.

The above analysis shows that all median city and nearshore WD_{10m} bias under the influence of TS, STS, and TY are clockwise, possibly in association with the biased representation of TC rotation in ERA5. The anticlockwise WD_{10m} bias for STY is indicative of deficient underlying surface roughness treatment, which could be also responsible for the large anticlockwise bias when TCs are within 100 km away from Shanghai (Figs. 9(a)–9(b)). The relatively larger nearshore WD_{10m} bias may imply an even poorer depiction of surface processes over the nearshore areas in ERA5. When TCs are beyond 100 km from Shanghai, the anticlockwise bias becomes smaller, but the clockwise bias increases. Dominant 10 m wind directions and bias distributions vary with TC tracks. In general, the difference of wind direction between ERA5 and AWS observations is small, which suggests that ERA5 captures the dominant wind direction reasonably well.

4.3 Upper-level wind speed

To assess how well ERA5 represents the upper-level wind, the wind fields at 26 levels from 975 to 100 hPa are compared against the sounding data at Baoshan station (Fig. 1). The radiosonde data, acquired at 08:00 and 20:00 Beijing Time each day, were matched to the closest ERA5 grid data at the same time. A total of 40 samples were obtained for the historical 16 TCs affecting Shanghai.

The median V_{upper} bias decreases with height, with a maximum value of 4.8 $m \cdot s^{-1}$ at 975 hPa (Fig. 11(a)). All the median biases below 900 hPa are positive, that is, ERA5 overestimates the wind speed, likely because ERA5 fails to fully represent the wind speed reduction effect of underlying urban rough surface. To some extent, it also reflects that the impact of surface friction can reach about 900 hPa. The biases between 900 and 300 hPa are rather small (< 1 $m \cdot s^{-1}$), and slightly increase above.

The V_{upper} MBE decreases with height for all TC categories and increases with TC intensity below 900 hPa (Fig. 11(c)). It is generally positive below 300 hPa, corresponding to an overestimate of wind speed, with an exception of the weakest TC category, TS, where the V_{upper} is underpredicted at most levels. Above 300 hPa, the V_{upper} MBE of all TCs is generally negative with weak vertical variations.

As shown in Fig. 11(e), when TC is located beyond 400 km south of Shanghai, the V_{upper} MBE below 900 hPa and between 700 and 300 hPa is positive, and negative at other levels. When TC is located at 200–400 km south of Shanghai, the V_{upper} MBE is mostly positive with a double peak at the surface and 400 hPa. When TC is within 200 km from Shanghai, the V_{upper} in ERA5 is biased low with a minimum MBE of –6.6 $m \cdot s^{-1}$ near 450 hPa. When TCs move to ~200 km north of Shanghai, the MBE below 600 hPa and above 300 hPa turns positive, but remains negative between 650 and 300 hPa. For TCs beyond 400 km north of Shanghai, the V_{upper} is biased high near the surface and low in the free atmosphere above.

The above analysis shows that, during the period of TC affecting Shanghai the V_{upper} bias decreases with height in the boundary layer. Below 900 hPa the V_{upper} in ERA5 is typically larger than the radiosonde observation, and its MBE increases with TC intensity. The result also indicates that ERA5 overestimates the V_{upper} above the boundary layer under the influence of STS, TY, and STY, but underestimates the observations for TS. Influenced by the TC wind structure, the V_{upper} MBE roughly presents a "M" type variation, that is, increasing first, followed by a decrease, then increasing and decreasing again with TC approaching and leaving Shanghai. Possibly due to the insufficient consideration of complex urban surface processes in ERA5, the near-surface V_{upper} is constantly overpredicted in ERA5. The dynamical impact of surface friction reaches 900 hPa for TCs beyond 100 km from Shanghai, decreasing to 925 hPa when TCs are within 100 km from Shanghai. In contrast, the MBE aloft displays a "negative——positive——negative——positive——negative" pattern, with relatively lager negative values for TCs within 100 km from Shanghai. The V_{upper} bias is mainly caused by the inability of ERA5 to accurately reproduce the TC structure, and the above results suggest that ERA5 may underestimate the high wind area and overestimate the low wind area. Additionally, previous studies (Liu et al., 2005; Chen, 2010) showed that the sounding balloon could undergo an obvious drift above 500 hPa, and the drifting usually increases with altitude, reaching ~0.5° at 150 hPa. Therefore, the balloon drifting should be partially contributed to the difference between EAR5 and radiosonde data.

4.4 Upper-level wind direction

The median WD_{upper} bias of ERA5 fluctuates around 0°, with a maximum of 6.7° only (Fig. 11(b)). The relatively larger variation range above 300 hPa is likely related to the balloon-drifting induced sounding data uncertainty. Below 300 hPa, the WD_{upper} MBE for TS (Fig. 11(d)) is positive, while it oscillates around 0° for other TC

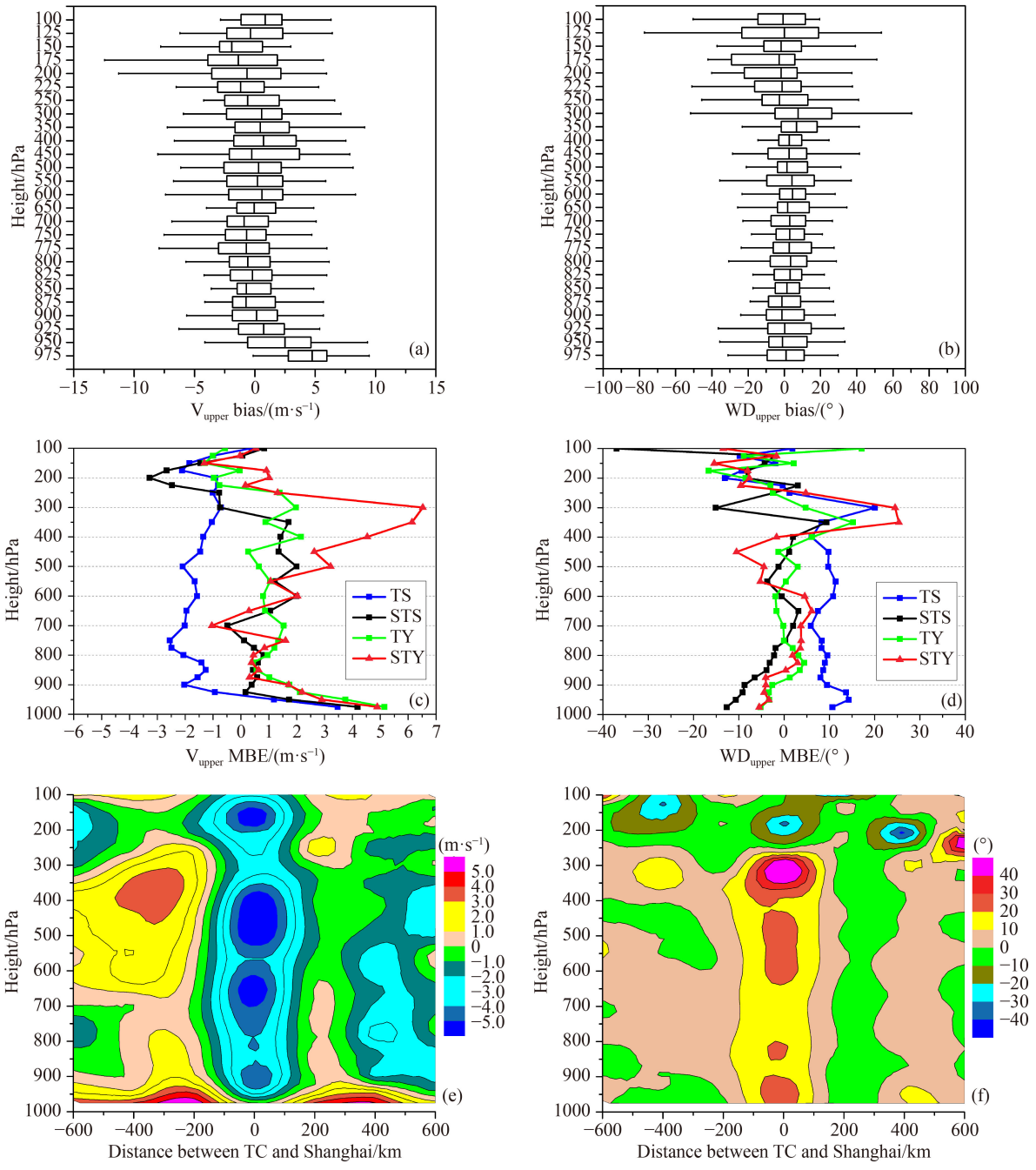

Fig. 11 Median V_{upper} and WD_{upper} bias (a)–(b), V_{upper} and WD_{upper} MBE (c)–(d) under the influence of TS, STS, TY, and STY, and V_{upper} and WD_{upper} MBE variations as a function of distance between TC and Shanghai (e)–(f). Negative and positive abscissa values in (e)–(f) indicate that TC is located to the south and north of Shanghai, respectively.

categories. Above 300 hPa, the WD_{upper} MBE is overwhelmingly negative, and is independent of both TC intensity (Fig. 11(d)) and its position with respect to the city (Fig. 11(f)). The WD_{upper} MBE below 300 hPa varies with the distance between TC and Shanghai (Fig. 11(f)), being positive with a maximum of 64° when TCs are within 200 km from Shanghai, while the WD_{upper} MBE alters roughly between −10° and 10° for TCs beyond 200 km away from Shanghai.

From the view of relative motion, the movement of TC approaching and leaving Shanghai can also be seen as the movement of Shanghai approaching and leaving TC. Thus, the sounding data in a TC event cover the whole TC structure. Therefore, the distribution of WD_{upper} with the distance from TC to Shanghai indicates that the cyclonic circulation within 200 km from the TC center in ERA5 generally lags behind, while the rotation out of 200 km from the TC center is close to observations. The WD_{upper} MBE in the upper troposphere is affected by the uncertainty of sounding data.

5 Conclusions and discussion

In this study, the TC best-track data of China Meteorological Administration and station observations are used to perform a systematic evaluation on the capability of ERA5 at representing TCs affecting Shanghai during 2007–2019, from the perspective of track, intensity, 10-m and upper-level wind. The main conclusions are as follows.

1) Corresponding to TS, STS, TY, STY, and SuperTY, the median TC track bias is 68.1, 52.9, 42.5, 25.4, and 18.2 km, respectively, the median $VMAX_{10m}$ bias is –3.7, –6.5, –11.4, –21.7, and –32.2 $m \cdot s^{-1}$, respectively, and the median $MSLP_{min}$ bias is 2.2, 5.6, 8.1, 28.2, and 48.7 hPa, respectively. With the increase of TC intensity, the median TC track bias decreases, while the median $VMAX_{10m}$ bias and $MSLP_{min}$ bias increase. The $VMAX_{10m}$ in ERA5 is generally lower than observations, while the $MSLP_{min}$ is usually higher than observations.

2) The median V_{10m} bias is 3.2, 4.2, 4.7, and 5.4 $m \cdot s^{-1}$ over the city, respectively, and is 4.4–5.2 $m \cdot s^{-1}$ over the nearshore area, respectively, corresponding to TS, STS, TY, and STY. The city V_{10m} bias increases with TC intensity, while the nearshore bias is larger and has no clear correlation with TC intensity. The bias features an "M" type trend with the distance between TC and Shanghai. When TCs are beyond 300 km from Shanghai, ERA5 overestimates V_{10m}, however, there are occasions where ERA5 underestimates V_{10m} when TCs are within 300 km from Shanghai, perhaps due to the ERA5's imperfect reproduction of the TC internal structure.

3) The median WD_{10m} bias is clockwise, with a value of 6.0°, 2.4°, 1.4° and –6.9° for the city and 0.8°, 5.7°, 6.5° and –0.7° for the nearshore region under the influence of TS, STS, TY, and STY. However, the anticlockwise median WD_{10m} bias for STY, which exceeds 20° when TCs are within 100 km from Shanghai, may indicate an insufficient consideration of urban surface processes in ERA5. When TCs is located beyond 100 km away from Shanghai, the anticlockwise bias is below 20°, and the clockwise bias is relatively larger. In addition, relatively smaller WD_{10m} biases are observed along the dominant wind direction.

4) The median V_{upper} bias generally decreases with height, and the influence of urban rough surface is detectable around 900 hPa. ERA5 typically overestimates the wind speed in the boundary layer, and the V_{upper} MBE increases with TC intensity. The V_{upper} bias is also modulated by the distance between TC and Shanghai. During the movement of TC approaching and leaving Shanghai, the V_{upper} MBE roughly undergoes an "M" type variation. Perhaps attributable to the deficient depiction of complex urban surface in ERA5, the V_{upper} MBE near surface is always positive. The V_{upper} MBE in the free atmosphere is characteristic of a "negative——positive——negative——positive——negative" pattern, with a relatively lager negative value for TCs within 100 km from Shanghai. These results suggests that ERA5 underestimates the high wind area but overestimates the low wind area of TC.

5) The WD_{upper} of ERA5 agrees well with the sounding data. The MBE above 300 hPa is generally negative. Below 300 hPa, the WD_{upper} MBE is positive for TCs within 200 km from Shanghai, while both positive and negative MBE are present for TCs beyond 200 km away from Shanghai, with a variation range of 10°. The variation pattern indicates that the cyclonic rotation within 200 km from the TC center in ERA5 lags behind, while the cyclonic circulation out of 200 km from the TC center is close to observations.

Similar to the previous findings of different reanalysis products, ERA5 underestimates TC intensity; the higher the TC intensity, the more significant the underestimate. A moderate bias in TC track exists as well, which decreases with TC intensity. In contrast to previous studies, this study focuses on the skill of ERA5 in representing the surface wind over the city and nearshore region and the upper-level wind under the influence of TCs. It should be noted that the upper-level wind is evaluated using instantaneous sounding data, which could induce in potential uncertainty to the conclusion. Anyway, our results would provide a useful reference for the application of ERA5 to study high impact weather in megacities. Future research will be extended to other meteorological fields, such as temperature, water vapor and surface precipitation associated with TCs, and other types of high impact weather, in order to provide a comprehensive evaluation of the performance of ERA5.

Acknowledgments This work was supported by the National Natural Science Foundation of China (Grant Nos. 41875059, 41875071, and 4175049), Shanghai Natural Science Foundation (No. 21ZR1457700).

References

An Y, Quan Y, Gu M (2013). Turbulence characteristics analysis of typhoon 'Mufia' near 500 m above ground in Lujiazui District of Shanghai. China Civil Eng J, 46(7): 21–27 (in Chinese)

Bian G, Nie G, Qiu X (2021). How well is outer tropical cyclone size represented in the ERA5 reanalysis dataset. Atmos Res, 249: 105339

Bosilovich M G , Santha A, Lawrence C, Richard C, Clara D, Ronald Ge, Robin K, Qing L, Andrea M, Peter N, Krzysztof W, Winston C, Rolf R, Lawrence T, Yury V, Steve B, Allison C, Stacey F, Gordon L, Gary P, Steven P, Oreste R, Siegfried D S, Max S (2015). MERRA-2: Initial evaluation of the climate. NASA Tech. Rep. Series on Global Modeling and Data Assimilation NASA/TM-2015-104606: 43

Chen Y, Han G, Jiao S, Wang Q, Yuan C (2008). Application of ECMWF products to typhoon track forecasting. J Meteor Sci, 28(2):

91–97 (in Chinese)

Chen Z (2010). Characteristics of the overall sounding data drift in China. Meteor Mon, 36(2): 22–27 (in Chinese)

Dee D P, Uppala S M, Simmons A J, Berrisford P, Poli P, Kobayashi S, Andrae U, Balmaseda M A, Balsamo G, Bauer P, Bechtold P, Beljaars A C M, van de Berg L, Bidlot J, Bormann N, Delsol C, Dragani R, Fuentes M, Geer A J, Haimberger L, Healy S B, Hersbach H, Hólm E V, Isaksen L, Kållberg P, Köhler M, Matricardi M, McNally A P, Monge-Sanz B M, Morcrette J J, Park B K, Peubey C, de Rosnay P, Tavolato C, Thépaut J N, Vitart F (2011). The ERA-Interim reanalysis: configuration and performance of the data assimilation system. Q J R Meteorol Soc, 137(656): 553–597

Geetha B, Balachandran S (2020). Development and rapid intensification of tropical cyclone OCKHI (2017) over the north Indian Ocean. J Atmosph Sci Res, 3(3): 13–22

Hart R E, Maue R N, Watson M C (2007). Estimating local memory of tropical cyclones through MPI anomaly evolution. Mon Weather Rev, 135(12): 3990–4005

Hatsushika H, Tsutsui J, Fiorino M, Onogi K (2006). Impact of wind profile retrievals on the analysis of tropical cyclones in the JRA-25 reanalysis. J Meteorol Soc Jpn, 84(5): 891–905

He L, Chen S, Guo Y (2020). Observation characteristics and synoptic mechanisms of typhoon Lekima extreme rainfall in 2019. J App Meteor Sci, 31(5): 513–526 (in Chinese)

Hersbach H (2019). ECMWF's ERA5 reanalysis extends back to 1979. ECMWF Newsl, No: 158

Hersbach H, Bell B, Berrisford P, Hirahara S, Horányi A, Muñoz-Sabater J, Nicolas J, Peubey C, Radu R, Schepers D, Simmons A, Soci C, Abdalla S, Abellan X, Balsamo G, Bechtold P, Biavati G, Bidlot J, Bonavita M, Chiara G, Dahlgren P, Dee D, Diamantakis M, Dragani R, Flemming J, Forbes R, Fuentes M, Geer A, Haimberger L, Healy S, Hogan R J, Hólm E, Janisková M, Keeley S, Laloyaux P, Lopez P, Lupu C, Radnoti G, Rosnay P, Rozum I, Vamborg F, Villaume S, Thépaut J N (2020). The ERA5 global reanalysis. Q J R Meteorol Soc, 146(730): 1999–2049

Hodges K, Cobb A, Vidale P L (2017). How well are tropical cyclones represented in reanalysis datasets? J Clim, 30(14): 5243–5264

Kobayashi S, Ota Y, Harada Y, Ebita A, Moriya M, Onoda H, Onogi K, Kamahori H, Kobayashi C, Endo H, Miyaoka K, Takahashi K (2015). The JRA-55 reanalysis: general specifications and basic characteristics. J Meteorol Soc Jpn, 93(1): 5–48

Knutson T R, Sirutis J J, Garner S T, Vecchi G A, Held I M (2008). Simulated reduction in Atlantic hurricane frequency under twenty first-century warming condition. Nat Geosci, 1(6): 359–364

Lam C C, Lai S T (1994). Use of ECMWF 850-hPa vorticity fields in the forecasting of tropical cyclones and intense lows in June-July 1994. In: Proceeding of 9th Guangdong-Hong Kong-Macau Joint Seminar on Hazardous Weather, Hong Kong Observatory, Hong Kong, China, 137–156

Liu H, Xue J, Shen T, Zhuang S, Zhu G (2005). Study on sounding balloon drifting and its impact on numerical predictions. J App Meteor Sci, 16(4): 518–526 (in Chinese)

Malakar P, Kesarkar A P, Bhate J N, Singh V, Deshamukhya A (2020). Comparison of reanalysis datasets to comprehend the evolution of tropical cyclones over North Indian Ocean. Earth Space Sci, 7(2): e2019EA000978

Maloney E, Hartmann D (2000a). Modulation of eastern North Pacific hurricanes by the Madden-Julian oscillation. J Clim, 13(9): 1451–1460

Maloney E, Hartmann D (2000b). Modulation of hurricane activity in the Gulf of Mexico by the Madden-Julian oscillation. Science, 287(5460): 2002–2004

Manning D M, Hart R E (2007). Evolution of North Atlantic ERA-40 tropical cyclone representation. Geophys Res Lett, 34(5): L05705

Murakami H (2014). Tropical cyclones in reanalysis data sets. Geophys Res Lett, 41(6): 2133–2141

Onogi K, Tsutsui J, Koide H, Sakamoto M, Kobayashi S, Hatsushika H, Matsumoto T, Yamazaki N, Kamahori H, Takahashi K, Kadokura S, Wada K, Kato K, Oyama R, Ose T, Mannoji N, Taira R (2007). The JRA-25 reanalysis. J Meteorol Soc Jpn, 85(3): 369–432

Rienecker M M, Suarez M J, Gelaro R, Todling R, Bacmeister J, Liu E, Bosilovich M G, Schubert S D, Takacs L, Kim G K, Bloom S, Chen J, Collins D, Conaty A, da Silva A, Gu W, Joiner J, Koster R D, Lucchesi R, Molod A, Owens T, Pawson S, Pegion P, Redder C R, Reichle R, Robertson F R, Ruddick A G, Sienkiewicz M, Woollen J (2011). MERRA: NASA's modern-era retrospective analysis for research and applications. J Clim, 24(14): 3624–2648

Saha S, Moorthi S, Pan H L, Wu X, Wang J, Nadiga S, Tripp P, Kistler R, Woollen J, Behringer D, Liu H, Stokes D, Grumbine R, Gayno G, Wang J, Hou Y T, Chuang H, Juang H M H, Sela J, Iredell M, Treadon R, Kleist D, Van Delst P, Keyser D, Derber J, Ek M, Meng J, Wei H, Yang R, Lord S, van den Dool H, Kumar A, Wang W, Long C, Chelliah M, Xue Y, Huang B, Schemm J K, Ebisuzaki W, Lin R, Xie P, Chen M, Zhou S, Higgins W, Zou C Z, Liu Q, Chen Y, Han Y, Cucurull L, Reynolds R W, Rutledge G, Goldberg M (2010). The NCEP climate forecast system reanalysis. Bull Am Meteorol Soc, 91(8): 1015–1058

Schenkel B A, Hart R E (2012). An examination of tropical cyclone position, intensity, and intensity life cycle within atmospheric reanalysis datasets. J Clim, 25(10): 3453–3475

Schenkel B A, Lin N, Chavas D, Oppenheimer M, Brammer A (2017). Evaluating outer tropical cyclone size in reanalysis datasets using QuikSCAT data. J Clim, 30(21): 8745–8762

Scoccimarro E, Gualdi S, Navarra A (2012). Tropical cyclone effects on Arctic Sea ice variability. Geophys Res Lett, 39(17): L17704

Thorne P W, Vose R S (2010). Reanalyses suitable for characterizing long-term trends: Are they really achievable? Bull Am Meteorol Soc, 91(3): 353–362

Tu S, Xu J, Chan J C L, Huang K, Xu F, Chiu L S (2021). Recent global decrease in the inner-core rain rate of tropical cyclones. Nat Commun, 12(1): 1948

Tu X, Yao R (2010). Analysis on ECMWF NWP products in track forecasting. J Trop Meteorol, 26(6): 759–764 (in Chinese)

Uppala S, KÅllberg P W, Simmons A J, Andrae U, Bechtold V D C, Fiorino M, Gibson J K, Haseler J, Hernandez A, Kelly G A, Li X, Onogi K, Saarinen S, Sokka N, Allan R P, Andersson E, Arpe K, Balmaseda M A, Beljaars A C M, Berg L V D, Bidlot J, Bormann N, Caires S, Chevallier F, Dethof A, Dragosavac M, Fisher M, Fuentes M, Hagemann S, Hólm E, Hoskins B J, Isaksen L, Janssen

P A E M, Jenne R, Mcnally A P, Mahfouf J F, Morcrette J J, Rayner N A, Saunders R W, Simon P, Sterl A, Trenberth K E, Untch A, Vasiljevic D, Viterbo P, Woollen J (2005). The ERA-40 re-analysis. Q J R Meteorol Soc, 131(612): 2961–3012

Wentz F J, Scott J, Hoffman R, Leidner M, Atlas R, Ardizzone J (2015). Remote sensing systems cross-calibrated multi-platform (CCMP) 6-hourly ocean vector wind analysis product on 0.25 deg grid, Version 2.0. Remote Sensing Systems, Santa Rosa, CA

Xi D, Han G, Yin X, Li Y, Liu Y, Tang Y (2020). Study on application of CPS method to typhoons affecting Jiangsu Province. Meteor Mon, 46(6): 765–775 (in Chinese)

Xu J (2005). Distribution of wind speed and direction when typhoons influencing Shanghai. Meteoro Mon, 31(8): 66–70 (in Chinese)

Ying M, Zhang W, Yu H, Lu X, Feng J, Fan Y, Zhu Y, Chen D (2014). An overview of the China Meteorological Administration tropical cyclone database. J Atmos Ocean Technol, 31(2): 287–301

Yue C, Tang Y, Gu W, Han Z, Wang X (2019). Study of city barrier effect on local typhoon precipitation. Meteor Mon, 45(11): 1611–1620 (in Chinese)

Zarzycki C M, Ullrich P A, Reed K A (2021). Metrics for evaluating tropical cyclones in climate data. J Appl Meteorol Climatol, 60(5): 643–660

Zick S E, Matyas C J (2015). Tropical cyclones in the North American regional reanalysis: an assessment of spatial biases in location, intensity, and structure. J Geophys Res D Atmospheres, 120(5): 1651–1669